Desalination and Water Treatment
www.deswater.com

doi: 10.1080/19443994.2013.844082

53 (2015) 794–805
January

Taylor & Francis
Taylor & Francis Group

Effect of metal ion (Zn^{2+}, Bi^{3+}, Cr^{3+}, and Ni^{2+})-doped CdS/halloysite nanotubes (HNTs) photocatalyst for the degradation of tetracycline under visible light

Weinan Xing[a], Liang Ni[a], Xinlin Liu[b], Yingying Luo[a], Ziyang Lu[a], Yongsheng Yan[a], Pengwei Huo[a,*]

[a]*Schools of Chemistry & Chemical Engineering, Jiangsu University, Zhenjiang 212013, P.R. China*
Tel. +86 51188790187; Fax: +86 51188791108; email: huopw@mail.ujs.edu.cn
[b]*School of Material Science and Engineering, Jiangsu University, Zhenjiang 212013, P.R. China*

Received 17 April 2013; Accepted 8 September 2013

ABSTRACT

CdS/halloysite nanotube (HNT) samples doped with several metal ions (M^{n+}-CdS/HNTs, where M^{n+} = Zn^{2+}, Bi^{3+}, Cr^{3+}, and Ni^{2+}) were synthesized using a facile and effective hydrothermal method. The as-prepared photocatalysts were characterized by scanning electron microscopy, transmission electron microscopy, X-ray energy dispersive spectroscopy, X-ray diffraction, UV–vis diffuse reflectance spectra, inductively coupled plasma-atomic emission spectroscope, X-ray photoelectron spectroscopy, and Fourier transform infrared. The photocatalytic activity of the M^{n+}-CdS/HNTs photocatalyst was evaluated by the degradation of tetracycline under visible-light irradiation. The optimum M^{n+}-doping amount was investigated in detail. At last, the possible photodegradation mechanism for metal-ion-doping photocatalyst was further discussed.

Keywords: Cadmium sulfide; Halloysite nanotube; Metal-ion doping; Photocatalysis; Tetracycline

1. Introduction

Photodegradation of waste water by various semiconductors is an effective technique for solving these current problems from environmental pollution. Among the various semiconductors used, CdS has been extensively studied because of its band gap (2.4 eV) and suitable conduction band potential, which can effectively absorb solar light [1,2]. However, photocorrosion of CdS is easy to occur during the photocatalytic reaction, so many methods like coupling CdS with other semiconductor compounds [3,4], supporting CdS with big mesoporous materials [5,6], embedding CdS particles in a polymer matrix [7,8], etc. have been used to improve the activity and stability of these catalysts.

Doping with metal ion is an effective method to improve the photocatalytic activity due to the separation of photogenerated electrons and holes. However, the choice of metal ion is a key problem. Based on the consideration of photocatalytic activities, normally noble metals such as platinum (Pt), palladium (Pd), and rhodium (Rh) [9,10] are a good choice. However, the higher cost greatly limits the standpoint of industrial application. It is necessary to develop other

*Corresponding author.

inexpensive metal ions. Some metal ions like Ni^{2+}, Sr^{2+}, and Cu^{2+} were also adopted by some researchers to improve the visible-light photocatalytic activity over CdS–ZnS solid solution photocatalysts [11–13].

Another strategy employed for enhancing the photocatalytic activity of photocatalyst is to disperse it on a support-like carbon nanotubes or graphene [14,15]. The dispersion of the photocatalyst produces can increase surface area by minimizing the aggregation of particles. However, the high cost and complex preparation of process had limited their practical applications. Halloysite nanotubes (HNTs) are a two-layered aluminosilicate clay mineral. They have hollow nanotube structure and large specific surface area. HNTs possess stabile property, resistible against organic solvents, and ease of disposal or reusability. More importantly, compared with other supported composites, HNTs are readily available and much cheaper [16,17]. HNTs have adequate hydroxyl groups on the surface of HNTs, which are potential anchoring sites for catalyst particles. Thus, we chose the HNTs as support.

Antibiotics are widely used as additives in animal medicine and feedstuff, which can enhance growth, control disease outbreak, and boost efficiency [18]. Along with the application of antibiotics, residues can be found in the environment and always result in environmental pollutions [19,20]. Among all the antibiotics, tetracyclines (TCs) are extensively used for disease control due to their great therapeutic values. Furthermore, the residues of TC have potential threaten to human. Therefore, it is necessary to treat and dispose the residues of TC in the waste water. In this study, we reported several metal ions such as Bi^{3+}, Ni^{2+}, Cr^{3+}, and Zn^{2+} which were doped into CdS/HNTs photocatalysts by the hydrothermal synthesis method. The as-prepared photocatalysts have been characterized by the scanning electron microscopy (SEM), transmission electron microscopy (TEM), X-ray energy dispersive spectroscopy (EDS), X-ray diffraction (XRD), UV–vis diffuse reflectance spectra (UV–vis DRS), Fourier transform infrared (FT-IR), inductively coupled plasma-atomic emission spectroscope (ICP-AES) and X-ray photoelectron spectroscopy (XPS). The photocatalytic activity of as-prepared photocatalysts was evaluated by the degradation of TC.

2. Experiment section

2.1. Materials

HNTs were purchased from the Zhengzhou Jinyang guang Chinaware Co., Ltd., Henan, China. Metal salts ($CdCl_2{\cdot}2.5H_2O$, $Zn(NO_3)_2{\cdot}6H_2O$, $Cr(NO_3)_3{\cdot}9H_2O$, $Ni(NO_3)_2{\cdot}6H_2O$ and $Bi(NO_3)_3{\cdot}5H_2O$) were all obtained from the Sinopharm Chemical Reagent Co., Ltd. (Shanghai, China) and used as received. Thiourea was obtained from the Shanghai Chemical Reagent Co., Ltd. TC was purchased from the Shanghai Shunbo Biological Engineering Co., Ltd. Deionized and doubly distilled water were used throughout this work.

2.2. Samples preparation

The M^{n+}-CdS/HNTs nanocatalysts were prepared via a simple hydrothermal synthesis method, which was similar to our previous study [21]. Briefly, HNTs (0.5 g) were added to 20.0 mL NaOH solution by ultrasonication for 10 min at room temperature to obtain HNTs suspension. Then, after a careful calculation, 10.0 mL of $CdCl_2{\cdot}2.5H_2O$ solution was dropped in 20.0 mL of the HNTs suspension while stirring. After 1 h, added into metal ion under stirring. The additional quantity of metal ion and $CdCl_2{\cdot}2.5H_2O$ was according to different molar ratios. At last, thiourea solution was added and then the mixture was transferred to a Teflon-lined stainless steel autoclave with a capacity of 50 mL, which was followed by a hydrothermal treatment at 160°C for 24 h. After cooling to room temperature, the precipitates were washed with deionized water and ethanol several times and dried at 60°C for 12 h. The obtained metal-doping CdS/HNTs photocatalysts were denoted by M^{n+}-CdS/HNTs ($M^{n+} = Zn^{2+}$, Bi^{3+}, Cr^{3+}, and Ni^{2+}). The M^{n+}-doping concentration was designed from 0 mol to 30 mol% (denoted as x mol% M^{n+}-doped CdS/HNTs, $x\ \text{mol\%} = [M/(M + Cd)] \times 100\%$).

2.3. Material characterization

The SEM images were examined by JSM-7001F scanning electron microscopy (JEOL Ltd., Japan). Elemental mapping over the selected regions of the photocatalyst was conducted by EDS. The TEM images were taken on a JEOL IEM-200CX TEM. The XRD patterns were obtained with a MO3XHF22 X-ray diffractometer (MAC Science, Japan) equipped with Ni-filtrated Cu Kα radiation (40 kV, 30 mA). The UV–vis diffuse reflectance spectra (UV–vis DRS) were obtained for the dry-pressed disk samples using a Specord 2,450 spectrometer (Shimazu, Japan) equipped with the integrated sphere accessory for diffuse reflectance spectra, using $BaSO_4$ as the reflectance sample. The FT-IR absorption spectra were obtained with a Nicolet Nexus 470 FT-IR (America thermo-electricity Company), using KBr pellets. XPS data were

recorded with a PHI5300 spectrometer using Al Kα (12.5 kV) X-ray source. A Varian Liberty150AX Turbo model, which was ICP-AES, was used for the determination of the metal ions concentration.

2.4. Measurement of photocatalytic activity

The photodegradation experiment of TC was carried out at 500 W in a GHX-2 photocatalytic reactor under a xenon lamp. In this part, a light filter (wavelength range 360–760 nm) was used in the photocatalytic reactor and less than 420 nm was removed by light filter. The photochemical reactor contained 0.1 g of catalyst and 30 mg/L of 100 mL TC aqueous solution. After 30 min in the dark, it reached absorption balance, and its initial absorbency was determined. The temperature of the reactant solution was maintained below 298 K by a flow of cooling water during the reaction. The reaction continued for 30 min and conducted in 5 min interval. It was determined at $\lambda_{max} = 357$ nm. The photocatalytic degradation rate (DR) was calculated by Eq. (1).

$$DR = [(1 - A_i/A_0)] \times 100\% \quad (1)$$

where A_0 is the initial absorbency of TC solution which reached absorption equilibrium and A_i is the absorbency of the reaction solution.

3. Results and discussion

3.1. SEM, EDS, and TEM analyses

The chemical composition and morphology of M^{n+}-CdS/HNTs were measured through EDS and SEM, respectively. As shown in Fig. 1, large amounts of nanoparticles were deposited on the surface of HNTs, which was the similar with our previous research. Fig. 1(b–e) displayed that the morphology of Bi^{3+}-CdS/HNTs, Ni^{2+}-CdS/HNTs, Cr^{3+}-CdS/HNTs, and Zn^{2+}-CdS/HNTs was similar with undoping photocatalyst, indicating that the doping has not influenced the morphology of M^{n+}-CdS/HNTs samples. From the EDS analysis, Bi, Ni, Cr, and Zn element can be clearly observed in M^{n+}-CdS/HNTs. The spectrum confirmed that the corresponding chemical elements were presented in the composite catalyst and indicated that no appreciable impurities were presented in the samples. As shown in Fig. 2, CdS exhibited nearly spherical, well-crystallized morphology. The nanoparticles were irregularly dispersed on the surface of HNTs.

3.2. ICP-AES analysis

ICP-AES was used for the determination of the metal ions concentration. The required pretreatment method of photocatalyst was as follows: 0.1 g sample was taken and dried, and then added into 5 mL aqua regia and 1 mL peroxide. After that, the mixture was heated to boiling and evaporating. Meanwhile, distilled water was added into the mixture to prevent it from drying out. At last, the mixture was centrifuged, and then the supernatant was taken and 10 mL distilled water was added. We used ICP-AES to detect the metal ions concentration and the results were shown in Table 1. It can be clearly seen that there were metal ions in the photocatalyst. Simultaneously, metal ions concentration of photocatalysts was increased along with the increase of the amount of metal ion during the preparation process of photocatalyst.

3.3. XRD analysis

To confirm that the crystal structure is retained intact for M^{n+}-CdS/HNTs as compared with undoping CdS/HNTs, powder XRD analysis was conducted. As shown in Fig. 3, all of these diffraction patterns were similar and can be assigned to CdS and HNTs, which had been reported before [21]. The sharp diffraction peaks indicated that the particles were fairly well-crystallized. The diffraction peaks of CdS can be indexed to hexagonal CdS according to the JCPDS No. 41−1049. All the patterns of the X-ray reflections of M^{n+}-CdS nanoparticles agreed with the hexagonal structure without any impurity phase. This evidently showed that the substitution of M^{n+} might have not affected the hexagonal structure. As the value of x increased, the diffraction peak also slightly changed, which was partially due to the M^{n+} incorporated into CdS and occupied the substitutional cationic sites.

3.4. UV–vis DRS analysis

UV−vis DRS was used to probe the optical absorption property and the band structure of materials. As shown in Fig. 4, all of the samples demonstrated excellent visible-light absorption. Fig. 4(A) shows the diffuse reflectance absorption spectra of Zn^{2+}-CdS/HNTs. It can be seen from Fig. 4(A) that there was a slight blue shift in the absorption edge with the increasing x. It may be due to the effect of different amount of Zn-ion doping. For a crystalline semiconductor, it is known that the optical absorption near the band edge follows (Eq. (2)).

$$ah = A(hv - E_g)^n \quad (2)$$

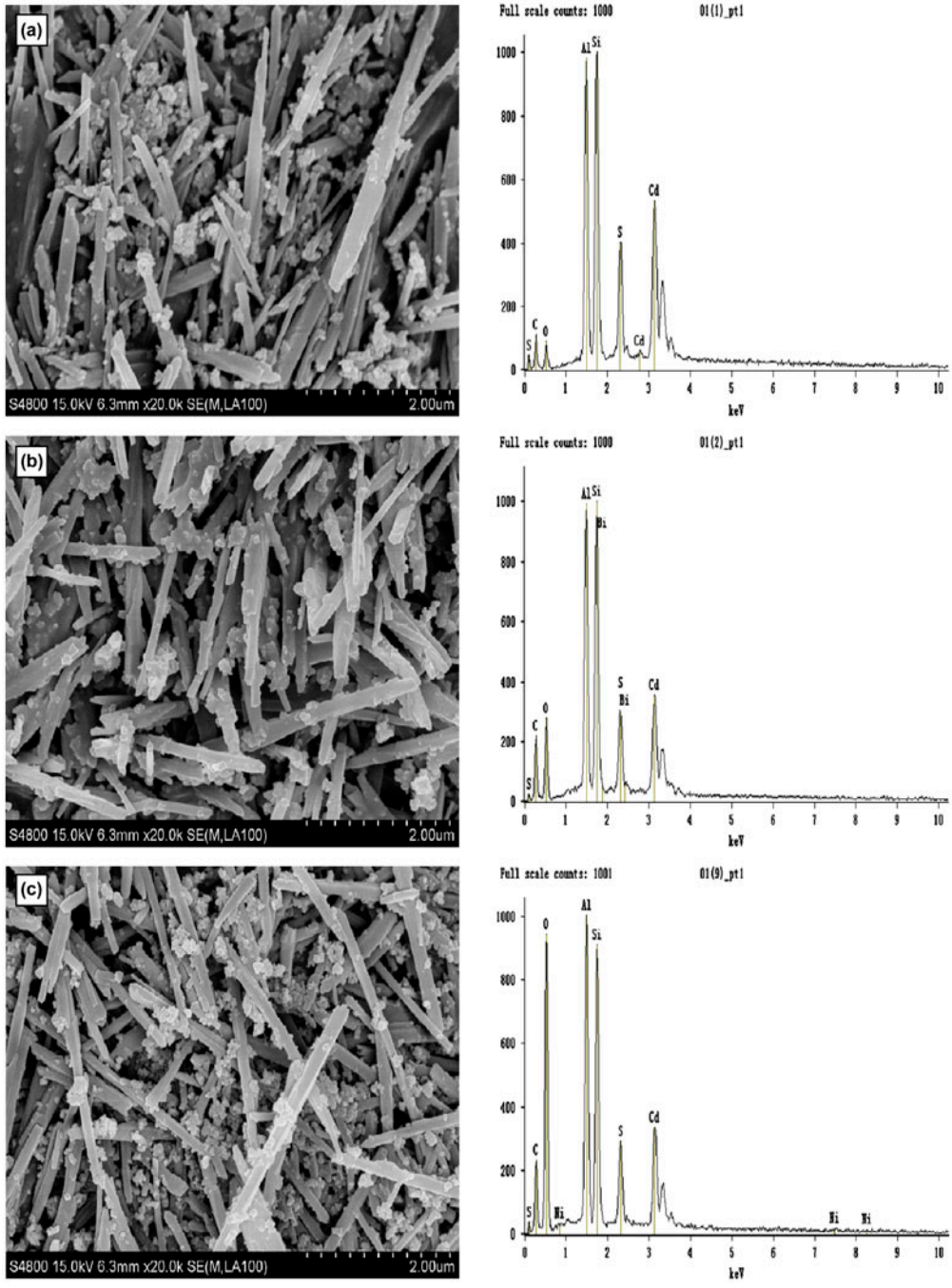

Fig. 1. SEM images and EDS spectrum of photocatalyst: (a) CdS/HNTs, (b) Bi^{3+}-CdS/HNTs, (c) Ni^{2+}-CdS/HNTs, (d) Cr^{3+}-CdS/HNTs, and (e) Zn^{2+}-CdS/HNTs.

where A is the probability parameter for the transition, hv is the incident photon energy, and n is the transition coefficient (1/2 for a direct transition or 2 for an indirect transition) [22]. The value of E_g can be directly estimated from a typical plot of $(ahv)^2$ vs. hv as shown in Fig. 4(E), and the band gap values estimated for these samples were in the range of 2.28–2.38 eV. With the increase of x, the band gap for Zn^{2+}-CdS/HNTs slightly and gradually increased. The UV–vis DRS spectra of Bi^{3+}-CdS/HNTs, Ni^{2+}-CdS/HNTs, and Cr^{3+}-CdS/HNTs, are shown in Fig. 4(B–D). The steep shape of the absorption edge of photocatalysts was about 550 nm. The doping has almost no influence on the absorption threshold

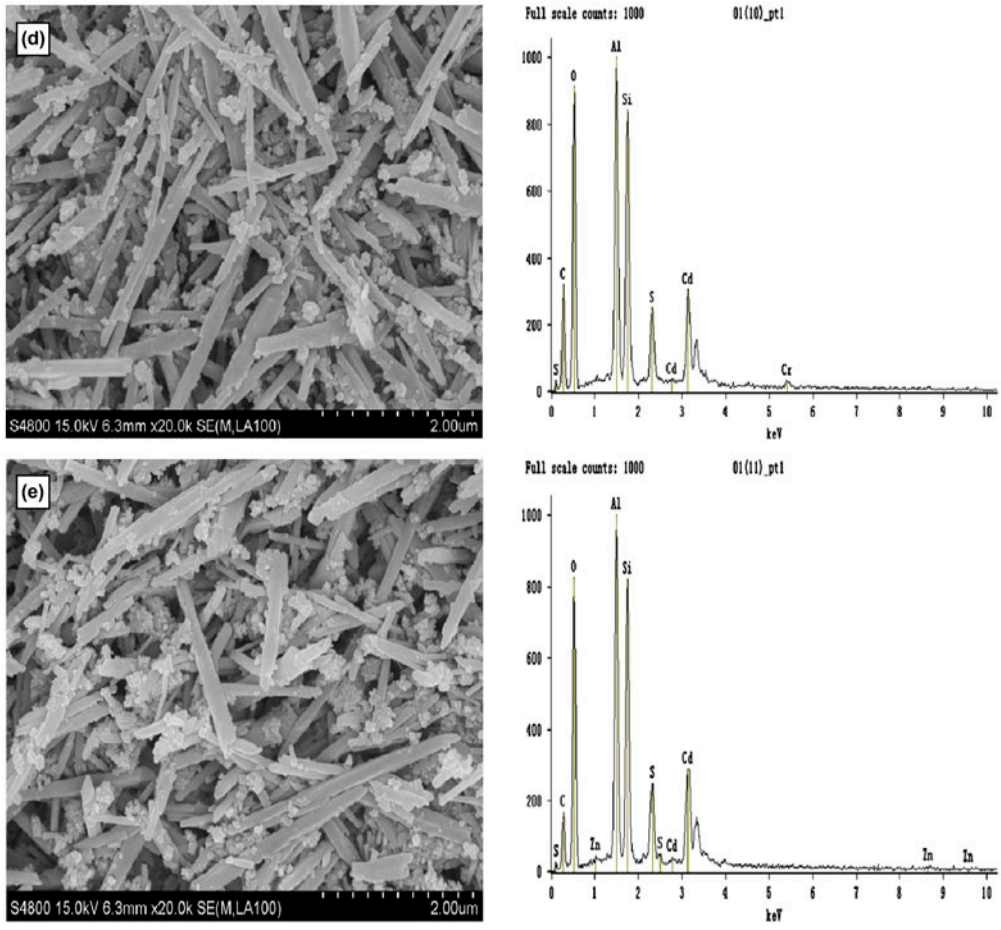

Fig. 1. (*Continued*).

values of the samples. In other words, M^{n+} doping did not markedly influence the band gap of CdS/HNTs. This phenomenon was also found in other researchers' reports, such as Sr-doping CdS–ZnS solid solution [12]. However, there was a very interesting phenomenon in Fig. 4(B–D), and the baselines of the doped samples elevate markedly with the increment of the M^{n+}-doping content. Such absorption was considered to attribute to the formation of impurity levels by the doping of metal ion, which was also found in the literature of Liu et al. [24].

3.5. XPS analysis

XPS analysis was performed to analyze the composition of the samples and the chemical state of the atoms. Fig. 5(A) shows the XPS spectra of Zn^{2+}-, Bi^{3+}-, Ni^{2+}-, and Cr^{3+}-CdS/HNTs photocatalysts. High resolution XPS spectrum Zn 2p of 30% Zn^{2+}-CdS/HNTs was shown in Fig. 5(B). The two peaks located at 1022.82 and 1046.23 eV were Zn 2p3/2 and Zn 2p1/2 in Zn^{2+}-CdS/HNTs photocatalyst, respectively, which slightly shifted toward higher energies compared to the values in database [23] and implied that the local chemical state was slightly influenced by Zn^{2+} incorporation into the CdS lattice. High resolution XPS spectrum Bi 4f of 30% Bi^{3+}-CdS/HNTs was shown in Fig. 5(C). The two peaks located at 161.85 and 153.59 eV were assigned to Bi 4f, and Si 2s. The peak of Bi 4f was a little different with the database, which may be the influence of overlap by the strong S 2p peaks [25]. As shown in Fig. 5(D), the two peaks located at 587.69 and 578.13 eV were assigned to Cr 2p, which were also slightly shifted toward higher energies compared to the values in database [23]. As shown in Fig. 5(A) (c) 30% Ni^{2+}-CdS/HNT photocatalyst, the main peak of Ni was overlapped with Cd MNN and the peaks could not be separated.

3.6. FT-IR analysis

The FT-IR spectra of photocatalysts were presented in Fig. 6. Two characteristic bands of HNTs at 3,695 and 3,620 cm^{-1} were presented intensely, which were

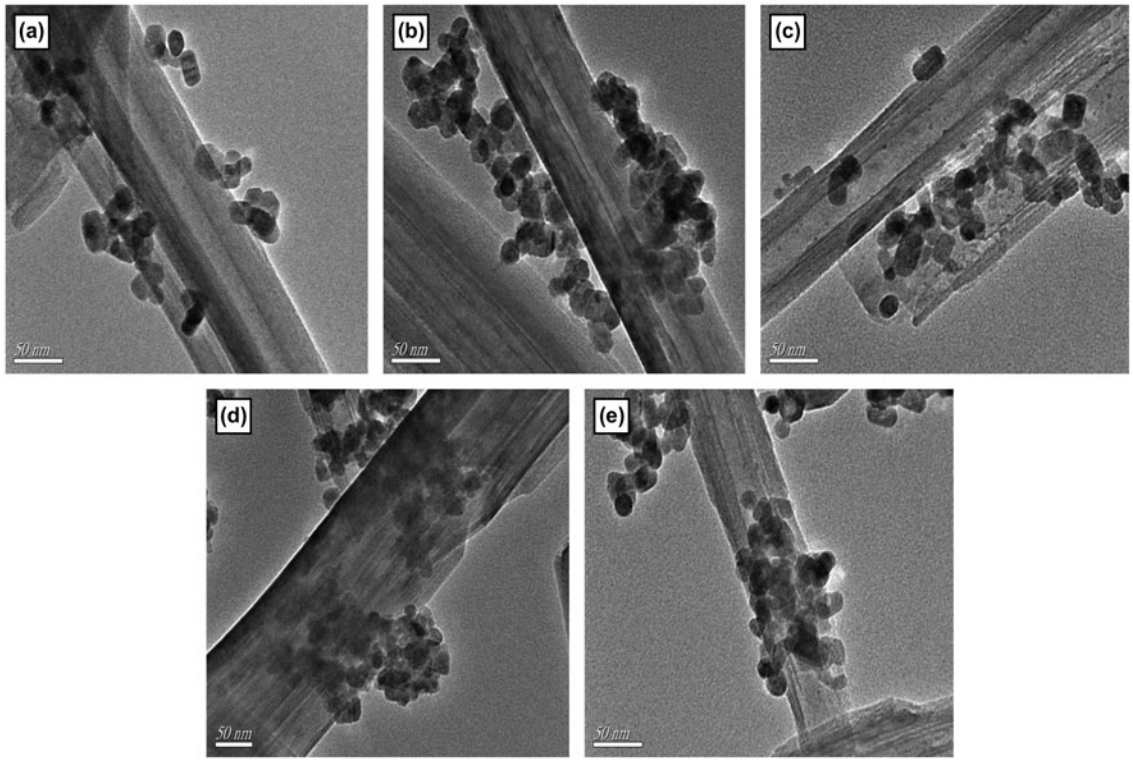

Fig. 2. TEM images of photocatalyst: (a) CdS/HNTs, (b) Bi^{3+}-CdS/HNTs, (c) Ni^{2+}-CdS/HNTs, (d) Cr^{3+}-CdS/HNTs, and (e) Zn^{2+}-CdS/HNTs.

due to the stretching vibrations of hydroxyl groups on the inner surface of HNTs. The Si–O groups in HNT exhibited the peak near 1,025 cm^{-1}. The peaks at 467, 536, and 910 cm^{-1} were attributed to the deformation

Table 1
Metal ions concentration of photocatalysts

Photocatalysts	Metal ions concentration (mg/g)				
	Cd^{2+}	Zn^{2+}	Bi^{3+}	Ni^{2+}	Cr^{3+}
Undoped CdS/HNTs	9.8332	0.019131	0.06578	0.024944	0.16153
1% Zn^{2+}-CdS/HNTs	10.148	1.7055	0.070249	0.036799	0.014656
5% Zn^{2+}-CdS/HNTs	10.314	0.74919	0.074967	0.0096391	0.012337
10% Zn^{2+}-CdS/HNTs	10.362	2.9521	0.084728	0.0066478	0.011109
30% Zn^{2+}-CdS/HNTs	10.072	5.6062	0.10343	0.0060852	0.009359
0.3% Bi^{3+}-CdS/HNTs	10.383	0.021803	0.41198	0.0077426	0.069551
0.6% Bi^{3+}-CdS/HNTs	10.497	0.013903	0.83512	0.0083555	0.013661
5% Bi^{3+}-CdS/HNTs	10.399	0.01373	7.2971	0.0070962	0.013812
30% Bi^{3+}-CdS/HNTs	9.7694	0.015812	11.226	0.0051581	0.011549
1% Ni^{2+}-CdS/HNTs	9.8166	0.017906	0.068532	1.6517	0.010976
5% Ni^{2+}-CdS/HNTs	10.037	0.032267	0.066819	3.7981	0.02238
10% Ni^{2+}-CdS/HNTs	10.293	0.041859	0.063198	4.5545	0.014347
30% Ni^{2+}-CdS/HNTs	9.9514	0.10034	0.045093	11.96	0.014027
1% Cr^{3+}-CdS/HNTs	9.8234	0.015826	0.065967	0.024944	0.52015
5% Cr^{3+}-CdS/HNTs	9.9305	0.014799	0.068422	0.0071131	1.189
10% Cr^{3+}-CdS/HNTs	10.072	0.013577	0.068685	0.032425	2.3244
30% Cr^{3+}-CdS/HNTs	9.874	0.017519	0.063011	0.0086144	6.9626

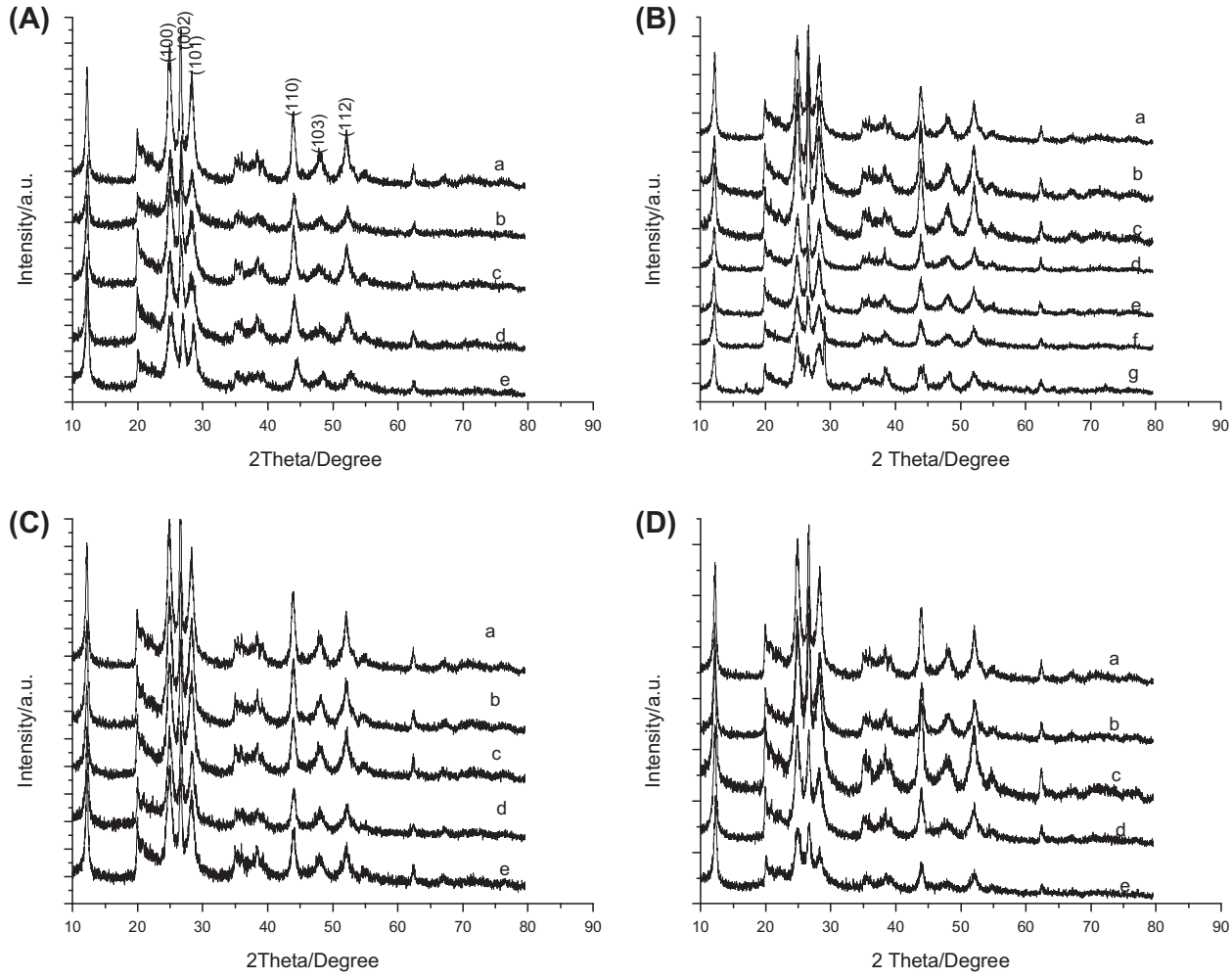

Fig. 3. XRD image of (A) Zn^{2+}-CdS/HNTs: (a) 0%, (b) 1%, (c) 5%, (d) 10%, and (e) 30%; (B) Bi^{3+}-CdS/HNTs: (a) 0%, (b) 0.3%, (c) 0.6%, (d) 1%, (e) 5%, (f) 10%, and (g) 30%; (C) Ni^{2+}-CdS/HNTs: (a) 0%, (b) 1%, (c) 5%, (d) 10%, and (e) 30%; and (D) Cr^{3+}-CdS/HNTs: (a) 0%, (b) 1%, (c) 5%, (d) 10%, and (e) 30%.

of Si–O–Si, Al–O–Si, and O–H of inner hydroxyl groups, respectively [21]. The above-mentioned peaks all appeared in FT-IR of M^{n+}-CdS/HNTs, while no other characteristic signals were existed. Therefore, metal-ion-doping CdS/HNTs may not have modified the structure of HNTs.

3.7. Photocatalytic activity

It is known that both the photocatalytic reaction and the simple physical adsorption have co-effects on the degradation of targets. In order to test the time at which the adsorption becomes balance, a dark adsorption experiment was carried out for 60 min. The absorption of different photocatalysts became balanced in 30 min as it was clear that the absorption rate was nearly invariable after that time. Hence, 30 min was chosen as the dark adsorption time in the photocatalysis experiment.

The photocatalytic activities of various samples were evaluated by the degradation of TC in aqueous solution under visible-light irradiation. In order to explore different photocatalytic activities of doping conditions, the degradation process of TC was studied using different doping mental ion photocatalysts. As we all know, metal-ion doping can act as a mediator of interfacial charge transfer or as a recombination center. Therefore, experiments were also carried out with different doping amounts to select the optimal value.

As shown in Fig. 7, all the samples, either doping or undoping, were active and stable for the photodegradation of TC. Zn^{2+}-CdS/HNTs photocatalysts showed enhanced activity compared to other doping

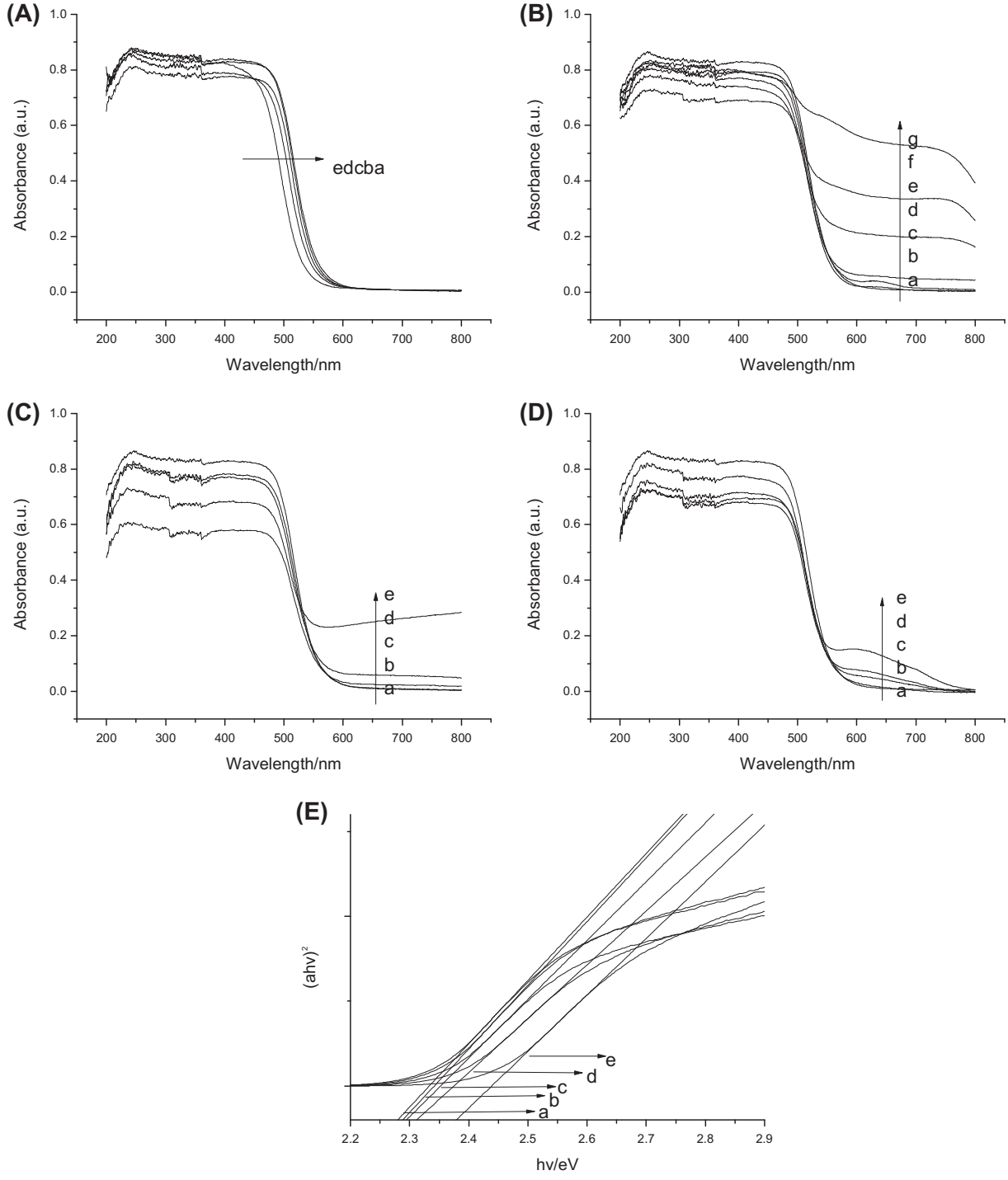

Fig. 4. UV−vis DRS of (A) Zn^{2+}-CdS/HNTs: (a) 0%, (b) 1%, (c) 5%, (d) 10%, and (e) 30%; (B) Bi^{3+}-CdS/HNTs: (a) 0%, (b) 0.3%, (c) 0.6%, (d) 1%, (e) 5%, (f) 10%, and (g) 30%; (C) Ni^{2+}-CdS/HNTs (a) 0% (b) 1% (c) 5% (d) 10% (e) 30%; (D) Cr^{3+}-CdS/HNTs: (a) 0%, (b) 1%, (c) 5%, (d) 10%, (e) 30%; and (E) band gap evaluation from the plots of $(Ahv)^2$ vs. photon energy(hv) Zn^{2+}-CdS/HNTs: (a) 0%, (b)1%, (c)5%, (d) 10%, and (e) 30%.

catalysts. It can be clearly seen that all the Zn^{2+}-CdS/HNTs samples showed relatively high photocatalytic activity than undoped photocatalyst for the photodegradation of TC. It was found that CdS/HNTs with 1% Zn^{2+} doped showed the highest activity for the photodegradation of TC. The DR could reach 92% in 30 min

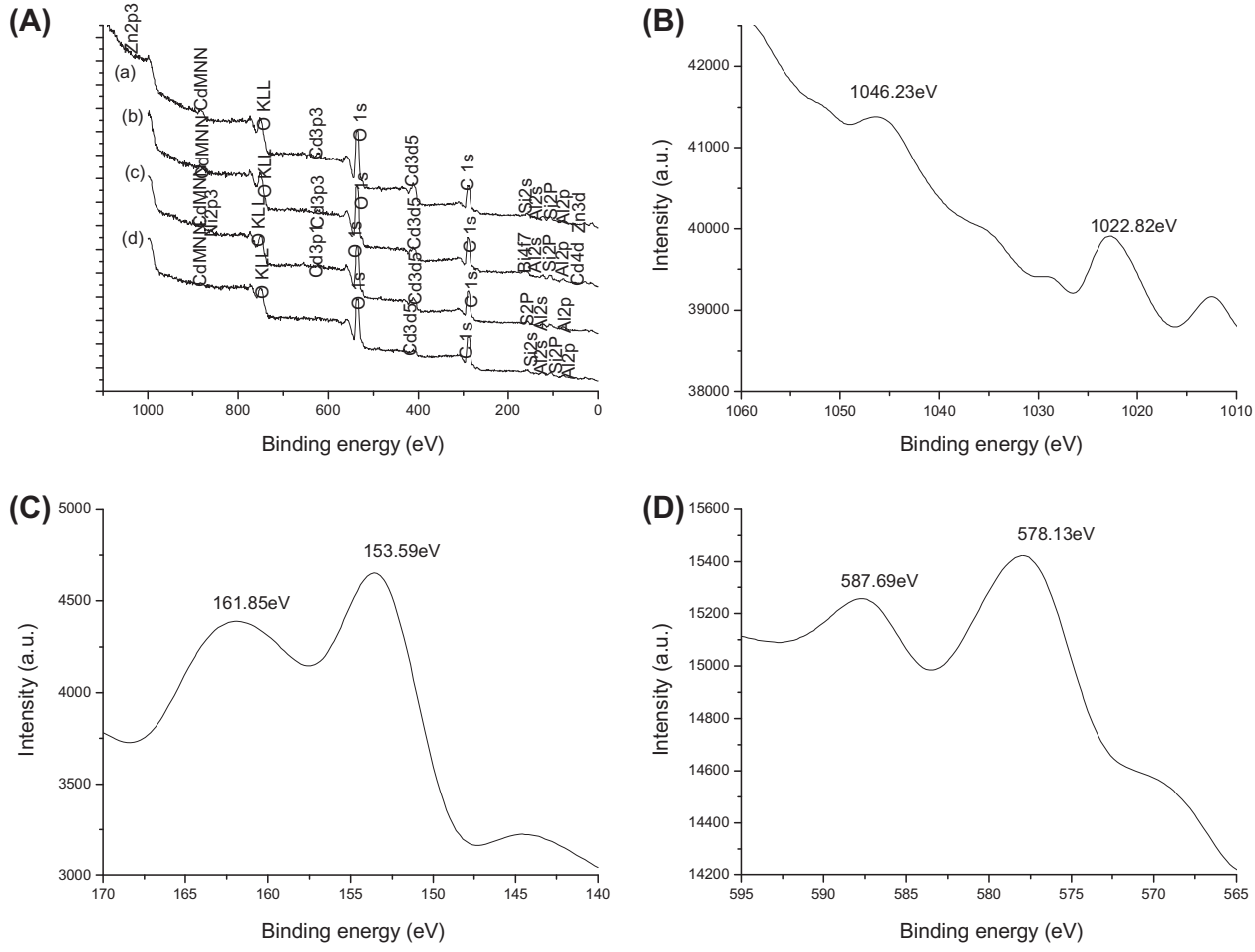

Fig. 5. (A) The XPS spectra of (a) 30% Zn^{2+}-CdS/HNTs, (b) 30% Bi^{3+}-CdS/HNTs, (c) 30% Ni^{2+}-CdS/HNT, and (d) 30% Cr^{3+}-CdS/HNTs. (B) High resolution XPS spectra Zn 2p of 30% Zn^{2+}-CdS/HNTs. (C) High resolution XPS spectra Bi 4f of 30% Bi^{3+}-CdS/HNTs. (D) High resolution XPS spectra Cr 2p of 30% Cr^{3+}-CdS/HNTs.

under visible-light irradiation. Further increase of Zn^{2+} content suppressed the photocatalytic activities. It is known that the addition of higher band gap catalyst (e.g. ZnS) to CdS decreases the extent of light absorbed, which was considered to be a disadvantage in terms of overall light absorption of the composite photocatalyst. This was corresponding to the result of UV–vis DRS analysis. However, the enlargement of the band gap by Zn^{2+} doping may be helpful for the enhancement of photocatalytic activities, because a larger band gap corresponds to more powerful redox ability. In this study, the highest photocatalytic activity was found 1% Zn^{2+}-CdS/HNTs, the appropriate amount of doped Zn^{2+}, leading to form a suitable band gap and a moderate position of conduction band.

Fig. 7(C–E) shows the photocatalytic activity of Bi^{3+}, Cr^{3+}, and Ni^{2+}-doped photocatalysts. It can be clearly seen that the highest photodegradation rate of Bi^{3+}-CdS/HNTs was 90%, which was close to Ni^{2+}-CdS/HNTs. Furthermore, the photodegradation

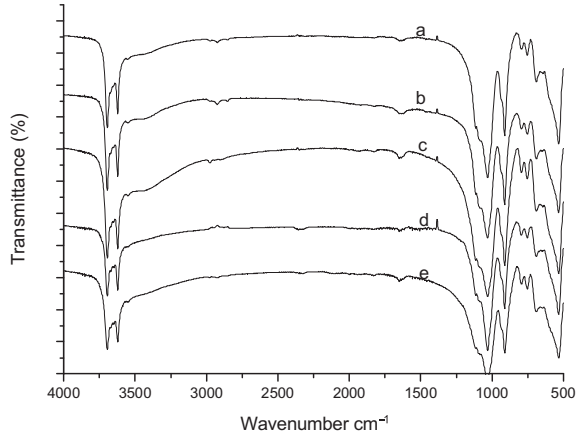

Fig. 6. FT-IR image of photocatalyst (a) CdS/HNTs, (b) Bi^{3+}-CdS/HNTs, (c) Ni^{2+}-CdS/HNTs, (d) Cr^{3+}-CdS/HNTs, and (e) Zn^{2+}-CdS/HNTs.

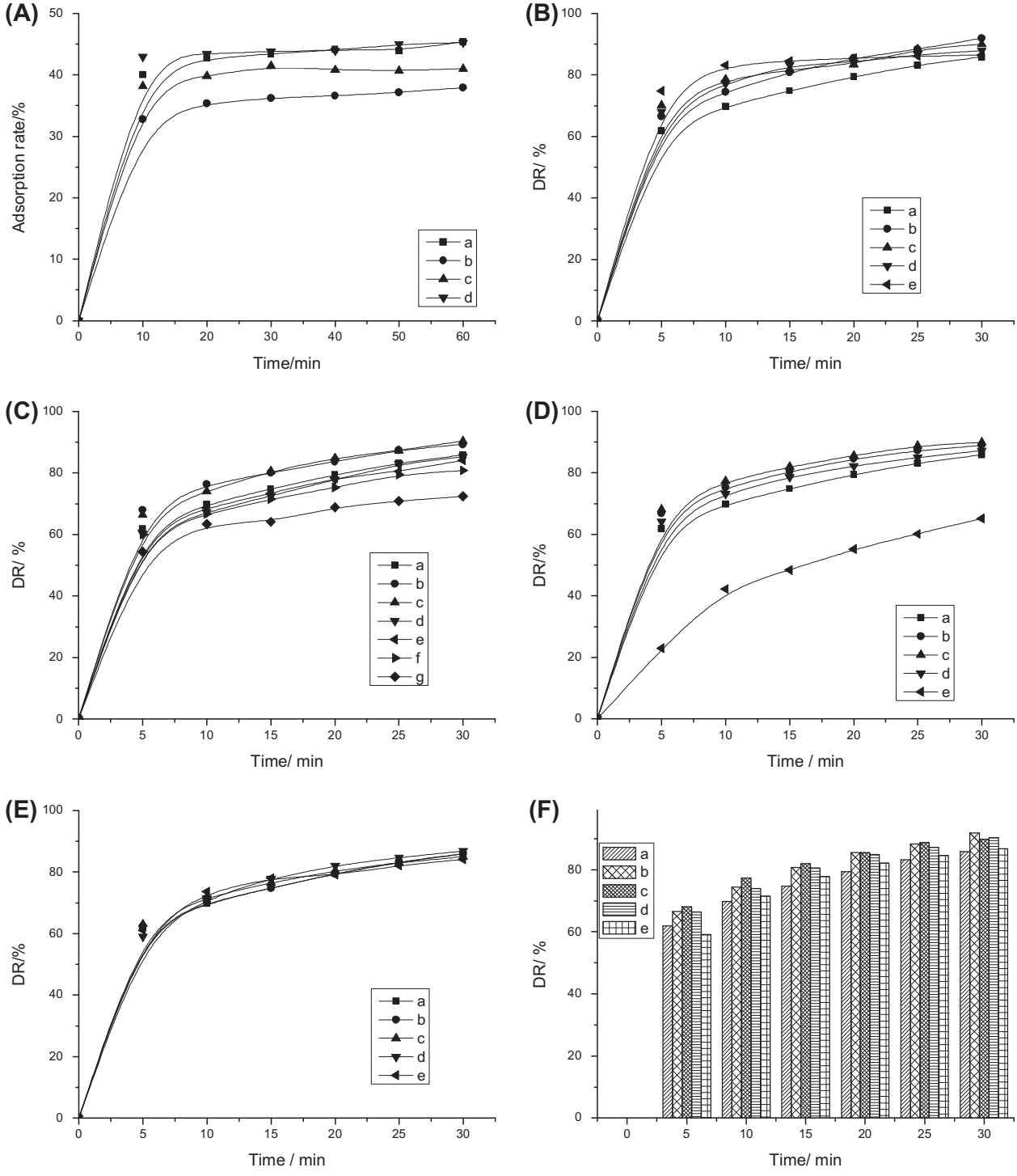

Fig. 7. (A) The adsorption rate of Bi^{3+}-CdS/HNTs (a) 1% (b) 5% (c) 10% (d) 30%. The degradation rate of different photocatalysts: (B) Zn^{2+}-CdS/HNTs: (a) 0%, (b) 1%, (c) 5%, (d)10%, and (e) 30%; (C) Bi^{3+}-CdS/HNTs: (a) 0%, (b) 0.3%, (c) 0.6%, (d) 1%, (e) 5%, (f) 10%, and (g) 30%; (D) Ni^{2+}-CdS/HNTs: (a) 0%, (b) 1%, (c) 5%, (d) 10%, and (e) 30%; (E) Cr^{3+}-CdS/HNTs: (a) 0%, (b) 1%, (c) 5%, (d) 10%, and (e) 30%; (F) (a) undoped CdS/HNTs, (b)1% Zn^{2+}-CdS/HNTs, (c) 5% Ni^{2+}-CdS/HNTs, (d) 0.6% Bi^{3+}-CdS/HNTs, and (e) 10% Cr^{3+}-CdS/HNTs.

rate of TC was increased along with the increasing doping amounts at the beginning, and then decreased at a higher doping amount which was lower than undoped photocatalyst. This result suggested that the

doping amount was an important factor to improve the photocatalytic activity. From the UV–vis DRS analysis, the presence of Bi^{3+}, Cr^{3+}, and Ni^{2+} ion did not significantly affect the band gap, indicating that the photocatalytic activities depended upon not only the visible-light absorption but also some other factors. On the basis of the predecessors' study, the possible reason for the changes of photocatalytic activities was the charge transfer. As we all know, metal-ion doping can serve as charge traps, retarding electron−hole combination rate and enhancing the interfacial charge transfer. Therefore, the photocatalytic activities improved. However, the photocatalytic activity was decreased at a higher doping amounts and even lower than undoped photocatalysts. It is because the surface atomic concentration of metal ion was too high, leading to the decrease of active sites at the surface of semiconductor, and then resulted in a lower activity. The comparison of photocatalytic activities of undoped CdS/HNTs and metal-ion-doping compounds is shown in this order (Fig. 6(F)): Zn^{2+}-CdS/HNTs > Bi^{3+}-CdS/HNTs ≈ Ni^{2+}-CdS/HNTs > Cr^{3+}-CdS/HNTs ≈ undoped CdS/HNTs.

3.8. Photodegradation mechanism

In the process of semiconductor photocatalytic degradation, mechanism investigation was an important part. According to the experimental results, the possible photodegradation mechanism for metal-ion-doping photocatalyst was presented as follows.

First, M^{n+}-CdS/HNTs photocatalyst was irradiated with photons of energy equal or greater than its band gap energy and the electron of the valence band became excited. Further, the excited electron jumped to the conduction band, and consequently the conduction band electrons and valence band holes were generated (3). Second, the formed e^- and h^+ pairs moved to catalyst surface, and then react with water and oxygen to create hydroxyl and superoxide radical anions [26] (4–5). Third, the OH· and other active radicals could effectively degrade the TC waste water (6).

$$\text{Metal sulfide} + h\nu \rightarrow e^- + h^+ \quad (3)$$

$$h^+ + H_2O \rightarrow H^+ + OH^\cdot \quad (4)$$

$$e^- + O_2 \rightarrow {}^\cdot O_2^- \quad (5)$$

$$TC + OH^\cdot \rightarrow CO_2 + H_2O + \text{other small inorganic molecules} \quad (6)$$

In general, the nanocrystal catalyst is meanwhile with serious recombination of the e^-/h^+ pairs due to large amounts of photogenerated charges (e^- and h^+) restricted in the small range [24]. Therefore, the separation rate of e^- and h^+ is an important process to improve the degradation rate. The introduction of doping M^{n+} in CdS/HNTs can illustrate the point best, because the doping M^{n+} on the shallow surface of photocatalyst can induce defects, which could serve as shallow trapping sites for electrons or holes. Such kind of shallow trapping can thus separate e^-/h^+ pairs at the surface, so as to greatly reduce their recombination on the surface of photocatalyst.

4. Conclusions

In summary, metal ion (Zn^{2+}, Bi^{3+}, Cr^{3+}, and Ni^{2+}) was doped into the CdS/HNTs for the first time by a simple hydrothermal method. The obtained Zn^{2+}–, Bi^{3+}–, and Ni^{2+}-CdS/HNTs photocatalyst showed higher photocatalytic activity for the degradation of tetracycline under visible-light irradiation, while Cr^{3+}-CdS/HNTs did not obviously perform improved activities. On the basis of the experiment and characterization results, the different effects of metal-ion doping on the photocatalytic activity were attributed to the confluence of the suppressed charge recombination of photon-generated carriers, the formation of a suitable band gap, and a moderate position of conduction band. On the other hand, M^{n+}-CdS/HNTs photocatalyst was economical compared with noble metal-doping photocatalyst. Therefore, it will have potential applications for the treatment and disposal the residues of TC from waste water.

Acknowledgments

We gratefully acknowledge the financial support of the financial support of the Natural Science Foundation of China (No. 21207053), the Natural Science Foundation of Jiangsu Province (SBK2011460), the Specialized Research Fund for the Doctoral Program of Higher Education (20113227110019), China Postdoctoral Science Foundation (2011M500861, 2012M511219, 2011M500869), and the program for Postgraduate Research Innovation in University of Jiangsu University (No. CXLX12_0634).

References

[1] H. Zhang, D. Yang, X.Y. Ma, Synthesis of flower-like CdS nanostructures by organic-free hydrothermal process and their optical properties, Mater. Lett. 61 (2007) 3507–3510.
[2] Y.Y. Huang, F.Q. Sun, T.X. Wu, Q.S. Wu, Z. Huang, H. Su, Z.H. Zhang, Photochemical preparation of CdS hollow microspheres at room temperature and their use in visible-light photocatalysis, J. Solid State Chem. 184 (2011) 644–648.

[3] Q. Zhu, J. Chen, M.G. Xu, S.W. Tian, H. Pan, J.S. Qian, X.F. Zhou, Microsphere assembly of rutile TiO_2 hierarchically hyperbranched nanorods: CdS sensitization and photovoltaic properties, Solid State Sciences 13 (2011) 1299–1303.
[4] J.W. Shi, X.X. Yan, H.J. Cui, X. Zong, M.L. Fu, S.H. Chen, L.Z. Wang, Low-temperature synthesis of CdS/TiO_2 composite photocatalysts: Influence of synthetic procedure on photocatalyticactivity under visible light, J. Mol. Catal. A: Chem. 356 (2012) 53–60.
[5] D. Barpuzary, Z. Khan, N. Vinothkumar, M. De, M. Qureshi, Hierarchically grown urchinlike CdS@ZnO and $CdS@Al_2O_3$ heteroarrays for efficient visible-light-driven photocatalytic hydrogen generation, J. Phys. Chem. C 116 (2012) 150–156.
[6] S.Y. Ryu, W. Balcerski, T.K. Lee, M.R. Hoffmann, Photocatalytic production of hydrogen from water with visible light using hybrid catalysts of CdS attached to microporous and mesoporous silicas, J. Phys. Chem. C 111 (2007) 18195–18203.
[7] Y.H. Yang, N. Ren, Y.H. Zhang, Y. Tang, Nanosized cadmium sulfide in polyelectrolyte protected mesoporous sphere: A stable and regeneratable photocatalyst for visible-light-induced removal of organic pollutants, J. Photochem. Photobiol. A 201 (2009) 111–120.
[8] H. Zhang, Y.F. Zhu, Significant Visible Photoactivity and Antiphotocorrosion performance of CdS photocatalysts after monolayer polyaniline hybridization, J. Phys. Chem. C 114 (2010) 5822–5826.
[9] A. Sathish, R.P. Viswanath, Photocatalytic generation of hydrogen over mesoporous CdS nanoparticle: Effect of particle size, noble metal and support, Catalysis Today 129 (2007) 421–427.
[10] H.J. Yan, J.H. Yang, G.J. Ma, G.P. Wu, X. Zong, Z.B. Lei, J.Y. Shi, C. Li, Visible-light-driven hydrogen production with extremely high quantum efficiency on Pt–PdS/CdS photocatalyst, J. Catal. 266 (2009) 165–168.
[11] M. Luo, Y. Liu, J.C. Hu, H. Liu, J.J. Li, One-pot synthesis of CdS and Ni-doped CdS hollow spheres with enhanced photocatalytic activity and durability, ACS Appl. Mater. Interfaces 4 (2012) 1813–1821.
[12] K. Zhang, D.W. Jing, Q.Y. Chen, L.J. Guo, Influence of Sr-doping on the photocatalytic activities of CdS–ZnS solid solution photocatalysts, Int. J. Hydrogen Energy 35 (2010) 2048–2057.
[13] M. Kimi, L. Yuliati, M. Shamsuddin, Preparation of Cu-doped Cd0.1Zn0.9S solid solution by hydrothermal method andits enhanced activity for hydrogen production under visible light irradiation, J. Photochem. Photobiol., A 230 (2012) 15–22.
[14] B. Liu, J.Y. Lee, Ordered alignment of CdS nanocrystals on MWCNTs without surface modification, J. Phys. Chem. B 109 (2005) 23783–23786.
[15] Z.Y. Gao, J.L. Liu, F. Xu, D.P. Wu, Z.L. Wu, K. Jiang, One-pot synthesis of grapheneecuprous oxide composite with enhanced photocatalytic activity, Solid State Sci. 14 (2012) 276–280.
[16] D. Papoulis, S. Komarneni, A. Nikolopoulou, P. Tsolis-Katagas et al., Palygorskite- and halloysite-TiO_2 nanocomposites: Synthesis and photocatalytic activity, Appl. Clay Sci. 50 (2010) 118–124.
[17] Y.F. Xie, D.Y. Qian, D.L. Wu, X.F. Ma, Magnetic halloysite nanotubes/iron oxide composites for the adsorption of dyes, Chem. Eng. J. 168 (2011) 959–963.
[18] I. Phillips, M. Casewell, T. Cox, B.D. Groot, C. Friis, R. Jones, C. Nightingale, R. Preston, J. Waddell, Does the use of antibiotics in food animals pose a risk to human health? A critical review of published data. J. Antimicrob. Chemoth. 53 (2004) 28–52.
[19] B.M. Marshall, S.B. Levy, Food animals and antimicrobials: Impacts on human health, Clin. Microbiol. Rev. 24 (2011) 718–733.
[20] F. Baquero, J.L. Martınez, R. Canton, Antibiotics and antibiotic resistance in water environments, Curr. Opin. Biotechnol. 19 (2008) 260–265.
[21] W.N. Xing, L. Ni, P.W. Huo, Z.Y. Lu, X.L. Liu, Y.Y. Luo, Y.S. Yan, Preparation high photocatalytic activity of CdS/halloysite nanotubes (HNTs) nanocomposites with hydrothermal method, Appl. Surf. Sci. 259 (2012) 698–704.
[22] J. Tauc, A. Menth, States in the Gap, J. Non-Cryst. Solids 8–10 (1972) 569–585.
[23] F. Yang, N.N. Yan, S. Huang, Q. Sun, L.Z. Zhang, Y. Yu, Zn-Doped CdS nanoarchitectures prepared by hydrothermal synthesis: Mechanism for enhanced photocatalytic activity and stability under visible light, J. Phys. Chem. C 116 (2012) 9078–9084.
[24] M.C. Liu, Y.C. Du, L.J. Ma, D.W. Jing, L.J. Guo, Manganese doped cadmium sulfide nanocrystal for hydrogen production from water under visible light, Int. J. Hydrogen Energy 37 (2012) 730–736.
[25] Y. Wang, Y. Wang, Y.L. Meng, H.M. Ding, Y.K Shan, A highly efficient visible-light-activated photocatalyst based on Bismuth- and Sulfur-codoped TiO_2, J. Phys. Chem. C 112 (2008) 6620–6626.
[26] L.W. Hou, H. Zhang, X.F. Xue, Ultrasound enhanced heterogeneous activation of peroxydisulfate by magnetite catalyst for the degradation of tetracycline in water, Sep. Purif. Technol. 84 (2012) 147–152.